Polymer 49 (2008) 2507–2514

Contents lists available at ScienceDirect

Polymer

journal homepage: www.elsevier.com/locate/polymer

The relationship between microstructure and toughness of biaxially oriented semicrystalline polyester films

YuanQiao Rao [a,*], Jehuda Greener [b], Carlos A. Avila-Orta [c], Benjamin S. Hsiao [d], Thomas N. Blanton [a]

[a] Research Laboratories, Eastman Kodak Company, Rochester, NY 14650-2109, United States
[b] Optical Display Films, Rohm and Haas Electronic Materials, Rochester, NY 14606, United States
[c] Departamento de Materiales Avanzados, Centro de Investigación en Química Aplicada, Boulevard Enrique Reyna H. No. 140, Saltillo, Coah, 25100, Mexico
[d] Department of Chemistry, State University of New York at Stony Brook, Stony Brook, NY 11794-3400, United States

ARTICLE INFO

Article history:
Received 4 January 2008
Received in revised form 11 March 2008
Accepted 15 March 2008
Available online 8 April 2008

Keywords:
Semicrystalline polyester
Toughness
Microstructure

ABSTRACT

The relationship between microstructure and toughness of biaxially stretched semicrystalline polyester films was investigated. Optically transparent films were prepared by simultaneous biaxial stretching of melt-cast sheets near the glass transition temperature. Copolyesters of polyethylene terephthalate (PET) with different compositions of two diols: ethylene glycol (EG) and cyclohexane dimethanol (CHDM), and stoichiometrically matched terephthalic acid were used to produce films with different degrees of crystallinity. In addition, the PET films with different crystalline morphologies were produced by constrained high temperature annealing of biaxially oriented films. The toughness, degree of crystallinity and crystalline morphology/molecular ordering were studied using mechanical testing, synchrotron small-angle X-ray scattering (SAXS), wide-angle X-ray diffraction (WAXD) techniques, and differential scanning calorimetry (DSC). The results indicate that the toughness of a semicrystalline polymeric film is determined by the interconnectivity of the crystalline phase within the amorphous phase and is greatly influenced by the degree of crystallinity and the underlying crystalline morphology.

1. Introduction

The ultimate mechanical properties of polymer films, such as toughness and tensile strength, are essential to a variety of applications. There have been theoretical attempts to calculate the ultimate strength based on material structure, e.g., the strength of a crystal can be calculated from its shear modulus [1]. However, most materials rarely follow the theoretical predictions, especially for ultimate properties that are sensitive to the presence of defects in the material. Therefore, phenomenological treatment such as the crack propagation measurement in fracture mechanics has proven to be more effective in providing insight into the material's behavior. Nevertheless, there is a growing need to design and synthesize materials from the bottom up to produce materials with desirable properties. For this reason, the fundamental understanding of the relationship between material structure and its ultimate properties, such as toughness, is particularly important.

Polymeric materials can pose special challenges with respect to the above problem because of their ill-defined molecular structure. Unlike most other materials, polymers possess covalently bonded long chains, which can assume an amorphous structure as well as ordered crystalline structure(s) when the crystallization enthalpy offsets the entropy penalty. These materials therefore can produce a large gamut of molecular structures, including amorphous, mesomorphic, and crystalline phases (with polymorphic arrangements) [2]. The crystalline–amorphous arrangements are usually in a lamellar form that resides within the spherullitic or fibrilar morphology [3], where the crystals have random or preferred orientation [4]. Extensive efforts have been devoted to understand the molecular structure and morphology of polymer systems and their relationship to mechanical properties. Notably, under tensile deformation, polymeric materials can undergo brittle-to-ductile transition with a change in temperature or in the presence of a notch, where yielding and brittle fracture modes often compete. The material typically yields during deformation if the molecules or the crystalline domains undergo conformational changes. Brittle fracture can be manifested by crack formation due to its inability to dissipate mechanical energy through conformational changes. Generally, amorphous polymers and highly crystalline polymers all exhibit brittle fracture and possess low toughness, whereas semicrystalline polymers show more complex fracture behavior because of the presence of both amorphous and crystalline phases [3]. As the detailed distribution, size and interconnectivity of the two phases have great influence on the fracture behavior of the

* Corresponding author. Tel.: +1 585 588 2609; fax: +1 585 477 7781.
E-mail address: yuanqiao.rao@kodak.com (YuanQiao Rao).

0032-3861/$ – see front matter © 2008 Elsevier Ltd. All rights reserved.
doi:10.1016/j.polymer.2008.03.046

material; understanding of this relationship is of great practical importance.

Polyethylene terephthalate (PET) is a semicrystalline polymer with broad applications, usually used in the form of fibers or films. PET films possess high stiffness, excellent dimensional stability and good optical transparency, and are widely used as transparent substrates, e.g., photographic films, transparencies, optical films in display applications. Typical PET film fabrication process involves biaxial stretching steps. In this study, we have employed a simultaneous biaxial stretching of quenched, melt-cast PET sheet at a temperature near its glass transition temperature to simulate the production process. During stretching, the initially amorphous sheet would develop strain-induced nanoscale crystals and a high degree of spatial arrangements and orientation for the integrated assembly of amorphous and crystalline phases. The structural changes during uniaxial stretching of PET have been studied quite extensively [5–17], but the study of the biaxial stretching process is less common.

In the uniaxial deformation study, it has been widely accepted that the PET molecules first form a mesomorphic state and then organize into lamellar crystals during the stretching step [7]. This hypothesis comes from the work of Yeh and Geil, who suggested that glassy PET is composed of granule-like structures, in which molecules possess a paracrystalline order [14,15]. During stretching, the paracrystalline structure can transform into lamellar crystals with tilted arrangement due to rotation and re-alignment. The pure mechanical properties and tensile behavior of biaxially stretched PET films have also been studied extensively. For example, semicrystalline PET films can undergo a ductile failure, where the nonlinear stress–strain behavior can be precisely modeled [18]. In particular, the fracture toughness of PET films can be thoroughly investigated by using the *J*-integral and essential work of fracture (EWF) methods [18–21]. Various structural characterization tools, such as infrared spectroscopy and intrinsic fluorescence, have been used to provide complementary molecular information about the deformation mechanisms of PET films [22–25].

However, in spite of extensive efforts to understand the ultimate mechanical properties of PET films, the fundamental knowledge of the relationship between microstructure and toughness is still not complete. The objective of this study is to shed further light on this relationship by using simultaneous synchrotron small-angle X-ray scattering (SAXS) and wide-angle X-ray diffraction (WAXD) techniques to monitor the structural change of a well-defined model sample under controlled deformation conditions. The microstructure relates to the crystalline morphology as well as the degree of crystallinity. The object of this study is to separate these two factors via two experiments: (a) keeping the same crystalline morphology but changing the degree of crystallinity of PET by adding a third comonomer and (b) changing the crystalline morphology by using a different heatset temperature during film processing.

2. Experimental

2.1. Materials

All the polyesters used in this study were obtained from Eastman Chemical Company. PET is a product of the condensation of two monomers: terephthalic acid (TA) and ethylene glycol (EG). A copolyester family containing an additional diol, cyclohexane dimethanol (CHDM), was also prepared (the copolyester is termed PET–CHDM). The PET–CHDM copolyester has the same diacid component as PET, terephthalic acid, but various compositions of the two diols: EG and CHDM. Table 1 lists all the resins used in this study. The level of CHDM in the copolymers was determined based on ^{1}H nuclear magnetic resonance spectroscopy (NMR). In order to generate additional polyester films with different controlled CHDM levels, blending of two polyesters (PET and CHDM-containing polyesters) with different CHDM content was necessary. Blending the two compositions was accomplished by drying each batch at 65 °C for 24 h and then extruding the dry blend at 277 °C using a twin-screw extruder.

Table 1
List of polyester resins with different diol compositions

Commercial tradename	Diol composition	
	EG, mol%	CHDM, mol%
PET 7352	100	0
PET 9921	96.5	3.5
PETG 6763	69	31
PCTG 5455	38	62
PCT A150	0	100

2.2. Polymer film preparation

2.2.1. Biaxial stretching

All biaxial films were prepared via a similar process. The crystallized resin was first dried at 160 °C for 12 h and then melt-extruded at 277 °C using a single screw extruder and a sheeting die. The molten resin was extruded onto an electrostatically charged casting drum at 43 °C to prepare an amorphous sheet with a thickness of about 1 mm. The cast sheet was then stretched biaxially. The biaxial stretching was done at ca. 105 °C by stretching 3–4 times in each direction. The thickness of the stretched film was ca. 80 μm.

2.2.2. Heatset

Some PET films were further heatset, i.e., annealed under lateral constraint at a temperature below the nominal melting point of the material. The annealing was done in a silicone oil bath at a given temperature for 10 s. The heatset temperatures varied from 150 to 230 °C.

2.3. Characterization techniques

2.3.1. Tensile toughness

All tests were performed in accordance with ASTM D 882-80a in a standard environment of 50% RH and 23 °C. The tensile test was conducted using a Sintech2 mechanical testing system with Testworks version 4.5 software. The specimen size was 1.5 cm wide by 10.2 cm long (gauge length). The crosshead speed was 5.1 cm/min. Five specimens were tested per film sample. The reported tensile toughness is the measured area under the stress–strain curve.

2.3.2. Differential scanning calorimetry (DSC)

DSC was used to measure the thermal behavior of the films. A Q1000 DSC (TA instruments) was used at a heating rate of 10 °C/min. Only first heating of the film was recorded. The enthalpy of the melting peak was used to calculate the degree of crystallinity, defined as:

$$X_c = \frac{\Delta H}{\Delta H_c} \times 100\% \quad (1)$$

where ΔH is the melting enthalpy of the sample calculated from the DSC data and ΔH_c is the melting enthalpy of a PET crystal (24.1 kJ/mol [32]).

2.3.3. X-ray scattering

Synchrotron small-angle X-ray scattering and wide-angle X-ray diffraction (SAXS and WAXD) measurements were carried out on beamlines X3A2 and X27C, respectively, at the National Synchrotron Light Source, BNL, Upton, NY. The wavelength and sample-to-detector distance at beamline X3A2 was 0.154 nm and 865.7 mm,

respectively, while for beamline X27C they were 0.137 nm and 119.6 mm, respectively. The collection time was 120 s for each measurement. Polyester films were cut into strips of 2 mm width in parallel and transverse directions with respect to the machine direction (MD). SAXS and WAXD measurements were collected along three different directions of the sample with respect to the machine direction: parallel direction (MD), transverse direction (TD) and normal direction (*d*).

3. Results and discussion

3.1. Effect of crystallinity on tensile properties of biaxially oriented PET–CHDM films

A series of PET–CHDM films with similar crystalline morphology but different crystallinity were generated. By using PET–CHDM copolyesters synthesized at different levels of CHDM and by blending the various copolyesters, the content of CHDM in the polyester film was varied from 0 to 62 mol% (hereafter, % CHDM means mol%). The films of different CHDM content were prepared using an identical process of biaxially stretching the cast amorphous film to a ratio of 3.2×3.5. These films were intentionally not heatset such that the effect of heatset, to be discussed later, is not considered in this discussion.

The XRD and DSC results suggest that crystallinity decreases with the incorporation of CHDM, when the level of the CHDM moiety is below 62% of the total diol content. The crystal structure of the crystals in this copolyester (below 62% CHDM) is the same as that of pure PET crystal based on the XRD data. Fig. 1 shows that the crystallinity of the biaxial PET–CHDM films decreases linearly with increasing level of CHDM (below 32%). The film is essentially amorphous when the CHDM concentration is in a range of 32–62%. The regressed relation between the crystallinity and CHDM (below 32%) can be expressed by:

$$X_{cr} = -1.1C_c + 38 \quad (2)$$

where X_{cr} is the degree of crystallinity, and C_c is the level of CHDM in mol%. The prefactor before C_c in Eq. (2) is simply a regression constant that apparently represents the effectiveness of disrupting PET crystals by the added CHDM comonomer.

Because CHDM is more rigid and bulky than EG, it does not fit in the unit cell of a PET crystal. Instead, it apparently creates a strain in the PET unit cell and therefore causes a decrease in crystallinity. It is known that the crystallinity of PET is greatly affected by how the sample is prepared. In the preparation of biaxial PET films, the

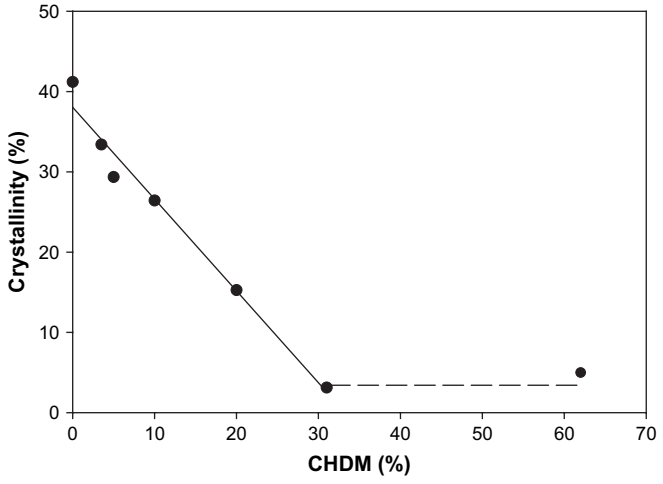

Fig. 1. Degree of crystallinity of PET-based polyesters vs. CHDM concentration; ● – experimental data, solid line is regression result for [CHDM] < 30 mol%.

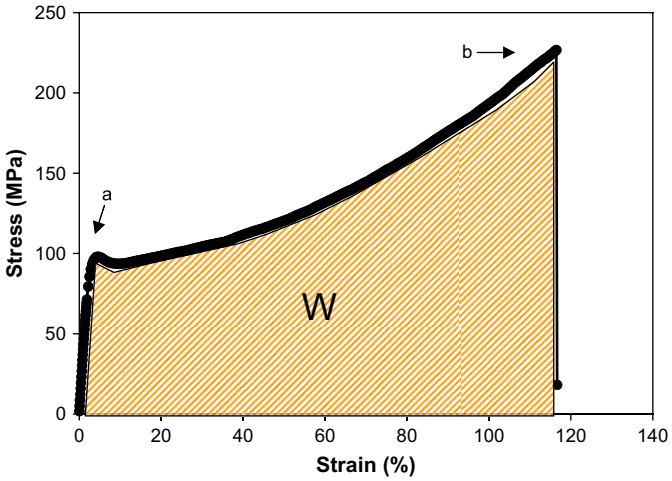

Fig. 2. Stress–strain curve for PET film heatset at 210 °C: a is the yield point, b is the break point and W (area under the curve) represents the tensile toughness.

cooling rate, the stretching temperature, the stretching ratio, and the final heatset temperature can change the level of crystallinity and crystalline morphology. Therefore, great care was taken in this study to assure that all the films of different CHDM content experience identical stress and thermal histories during processing. A general stress–strain curve of a PET–CHDM film is shown in Fig. 2. It is noted that the PET–CHDM film undergoes a ductile failure. The material yields at ca. 2% elongation following by strain hardening and a catastrophic failure at the break elongation point. The tensile toughness is the area under the stress–strain curve. All the tensile properties, i.e., Young's modulus, the yield stress, the break strength, and the elongation to break, affect the toughness. Table 2 lists the mechanical properties of the PET–CHDM films at different CHDM levels. It is seen that in general the Young's modulus, yield stress, break strength, and elongation to break decrease with increasing CHDM level. However, the extent of decrease is different. The Young's modulus and the yield stress decrease approximately linearly, while the tensile strength and elongation to break decrease more rapidly with CHDM. The X-ray diffraction (XRD) data suggest no change in the crystal structure upon variation of the CHDM level within the range of 0 to 62 mol% (Fig 1). It is hypothesized that randomly oriented lamellar crystal sheets based on the chain-extended structure are formed during biaxial stretching [26,27]. The stress–strain behavior of PET–CHDM in the ductile ("plastic flow") regime appears to control the toughness of the film, which can be understood by the following argument. It is well known that the modulus of the oriented film is largely controlled by the state of orientation of the amorphous and crystalline phases while the crystallinity only has a limited effect on the modulus [28]. However, the ultimate properties, i.e., the tensile strength and the elongation to break, can be significantly modified by the degree of crystallinity and crystal morphology. The crystalline domains typically act as physical "crosslinks" that increase the resistance of the material to configurational changes and relative chain sliding at high deformations, thus increasing the yield stress, break strength,

Table 2
Mechanical properties of PET–CHDM films

CHDM fraction, %	Young's modulus, GPa	Yield strength, MPa	Break strength, MPa	Break elongation, %
0	4.2 (0.2)	72 (2)	179 (14)	130 (6)
3.5	3.3 (0.1)	72 (4)	165 (9)	115 (15)
10	3.3 (0.1)	69 (0)	124 (0)	90 (2)
20	2.8 (0.2)	54 (6)	112 (27)	99 (14)
31	2.7 (0.2)	60 (1)	117 (1)	83 (13)
62	2.8 (0.2)	67 (1)	123 (1)	73 (13)

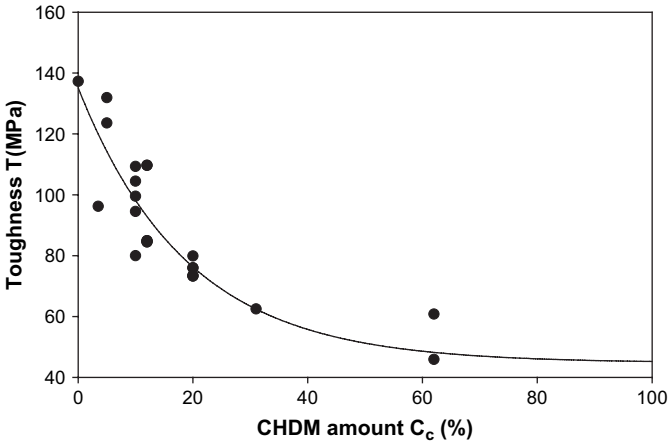

Fig. 3. Toughness vs. CHDM concentration in biaxially oriented PET–CHDM films: dots are experimental data; curve is the regression result.

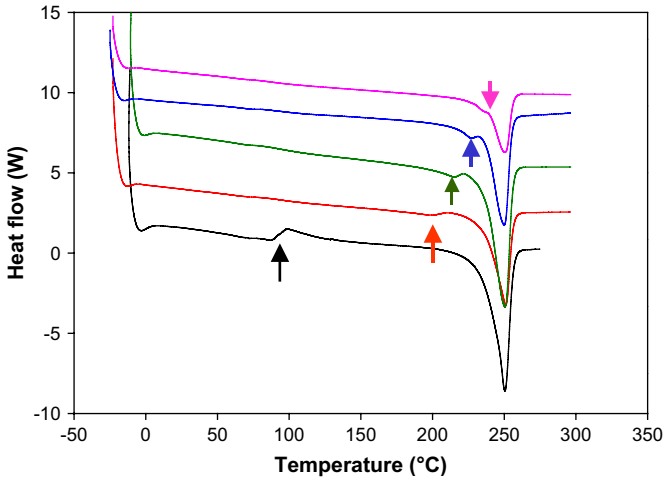

Fig. 4. DSC thermograms for PET films heatset at various temperatures; from bottom to top: non-heatset, 196 °C, 215 °C, 227 °C, and 236 °C.

and elongation to break. Fig. 3 shows the effect of CHDM level on the toughness of the PET–CHDM film. This effect can be expressed by the following relationship obtained by regression:

$$T = 44.8 + 90.4\,e^{-0.05C_c} \quad (3)$$

When $C_c < 30$ mol%, Eq. (3) can be simplified as:

$$T = 135 - 2.7C_c \quad (3a)$$

where T is toughness in MPa and C_c is the level of CHDM in mol%. By combining Eqs. (2) and (3), it is possible to correlate the toughness of PET–CHDM films with crystallinity. The results suggest the existence of a critical crystallinity threshold, above which significant enhancement in tensile properties can be achieved.

3.2. *Effect of crystalline morphology on the toughness of biaxially oriented PET films*

In the previous section, it is shown that the incorporation of a different chemical moiety to the polymer chain affects the crystallization behavior as well as the mechanical properties of PET films. The film process is also expected to change the structure and properties of PET films. Heatsetting of semicrystalline films and corresponding structural changes have been studied quite extensively [29–31]. In these studies, increase in crystallinity and size of the crystalline domains were generally observed upon heatsetting of biaxially oriented semicrystalline polymer films. Another interesting finding was the existence of the fibrillar-to-lamellar transformation at a critical heatset temperature below the nominal melting point of the film [29,30]. To further elucidate this phenomenon, heatsetting experiments were conducted in an attempt to relate the microstructure to the toughness. The observed unit cell parameters were consistent with typical reported values for PET [4], i.e., a triclinic cell with $a = 4.59$, $b = 5.94$, and $c = 10.75$ Å, and the chain axis parallel to the c-axis. PET has a nominal melting point of 265 °C (and heat of fusion of 24.1 kJ/mol [32]), and in this study the heatsetting temperatures ranged from 30 to 100 °C below the melting point. Fig. 4 shows the DSC scans of PET films heatset at different temperatures. In the DSC thermogram for the non-heatset biaxially stretched sample, an endotherm at ca. 105 °C, which coincides with the stretching temperature of the film, is seen. For the heatset biaxially stretched samples, two features are observed. First, a major melting peak can be found at 251 °C (±0.5 °C) for all heatset temperatures, but the corresponding melting enthalpy varies among the various samples. This melting endotherm is due to the melting of "primary" crystals generated by strain-induced crystallization during the biaxial stretching process. Second, a new ("secondary") melting endotherm is seen for all heatset films, where the corresponding peak temperature coincides with the applied heatset temperature (indicated by the arrows in Fig. 4). This has also been reported in an earlier study, where the two melting peaks in the heatset films have been attributed to two distinct morphologies [27,29]. It is noted that the secondary melting temperature is significantly lower than the primary melting temperature. There are several possible mechanisms for the development of the secondary melting endotherm, e.g., crystals of different unit cells induced by tension and heatsetting, strained crystals due to taut chains, and secondary crystals of small size (see Ref. [29] for complete discussion of this point). As the detailed XRD data from the heatset samples did not reveal a new crystal unit cell, the first possibility can be ruled out but the other two possibilities are likely valid. During the heatsetting process, the oriented amorphous taut chains would gain mobility due to the influx of thermal energy. Since the material is constrained in the lateral directions, the mobile chains can form new secondary crystals in the direction perpendicular to the film plane, along which the mobility is not restricted. The secondary crystals are generally smaller in size and also have lamellar morphology with crystal orientation perpendicular to chain-extended crystals formed during stretching. The existing chain-extended crystals confine the newly formed secondary crystals, and they will melt first because of the small size resulting in the lower melt temperature endotherm.

The toughness of the heatset films was measured and correlated with the microstructure of the films. The effect of heatset temperature on the toughness and the degree of crystallinity is illustrated in Fig. 5. It is seen that the crystallinity of the PET films increases at low heatset temperatures and then decreases above a critical temperature of about 228 °C (i.e., ca. 25 °C below its nominal melting temperature). The toughness is also seen to undergo a maximum with the heatset temperature with the maximum toughness being ca. 60% higher than the toughness of non-heatset film. The increase in toughness may be partially attributed to the increased crystallinity but further examination of the data suggests that other factors such as morphology and microstructure could also make a contribution. This becomes quite clear when the toughness is plotted against the degree of crystallinity as shown in Fig. 6. The results from two sets of films are illustrated in this figure. One set includes the PET–CHDM films discussed earlier, where samples were prepared at different CHDM levels under the same stretching conditions without heatsetting, resulting in different degrees of crystallinity. Another set covers the PET films heatset at

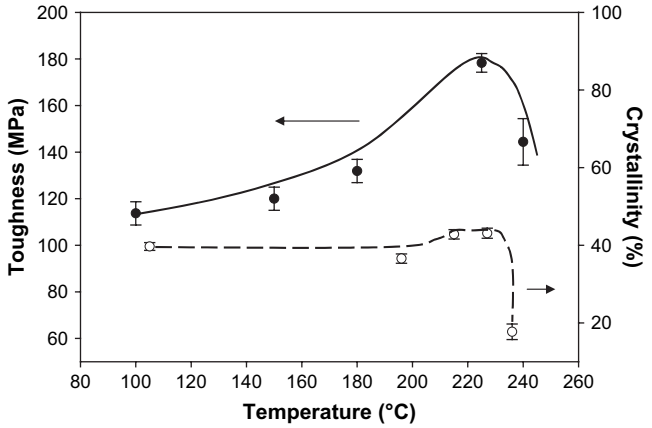

Fig. 5. Toughness and degree of crystallinity vs. heatset temperature in biaxially oriented PET films.

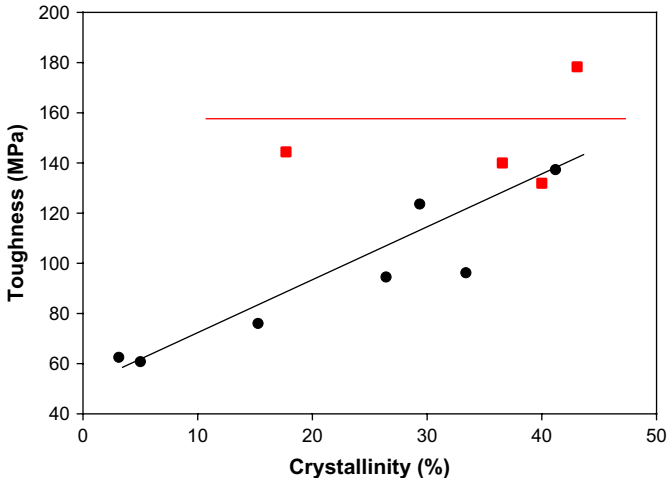

Fig. 6. Toughness vs. degree of crystallinity: (●) PET–CHDM films at various CHDM levels; (■) PET films heatset at various temperatures.

different temperatures following biaxial stretching. A clear correlation between the toughness and the crystallinity is observed in the PET–CHDM films, whereas the correlation between the toughness and the crystallinity is not as clear in the case of the PET films. This finding prompted us to carry out a more in depth investigation of the microstructure and its impact on the toughness of the film.

2D SAXS and WAXD patterns were collected from three orthogonal directions (MD: machine direction; TD: transverse direction; *d*: thickness direction or neutral direction) of biaxially stretched PET films. The images (SAXS and WAXD) taken along the two plane directions (i.e., normal to the MD–*d* plane and normal to the TD–*d* plane) are highly oriented and look similar, whereas the image taken normal to the film plane (i.e., the MD–TD plane) is near isotropic. These scattering/diffraction features are typical from biaxially stretched PET films. The near isotropic scattering/diffraction pattern (normal to the film plane) is a good indication of near symmetric stretching.

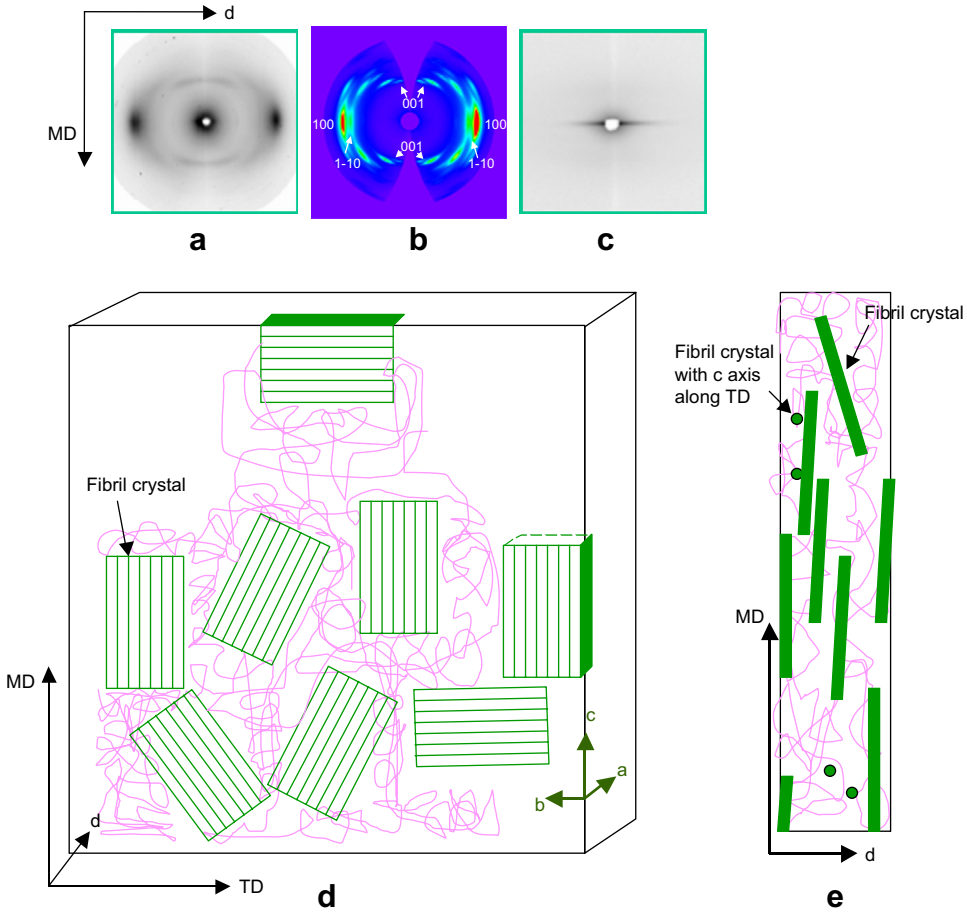

Fig. 7. Microstructure of biaxially stretched PET film: (a) WAXD pattern; (b) indexing of WAXD pattern; (c) SAXS pattern; (d) 3-D microstructure of PET film, random fibril crystals randomly distribute in the MD–TD plane; (e) thin crystal sheets seen in the MD–*d* plane and the dots represent crystals whose *c*-axes are along TD direction. The X-ray incident along the TD direction and normal to the MD–*d* plane, where TD is transverse direction, MD is machine direction and *d* is thickness direction.

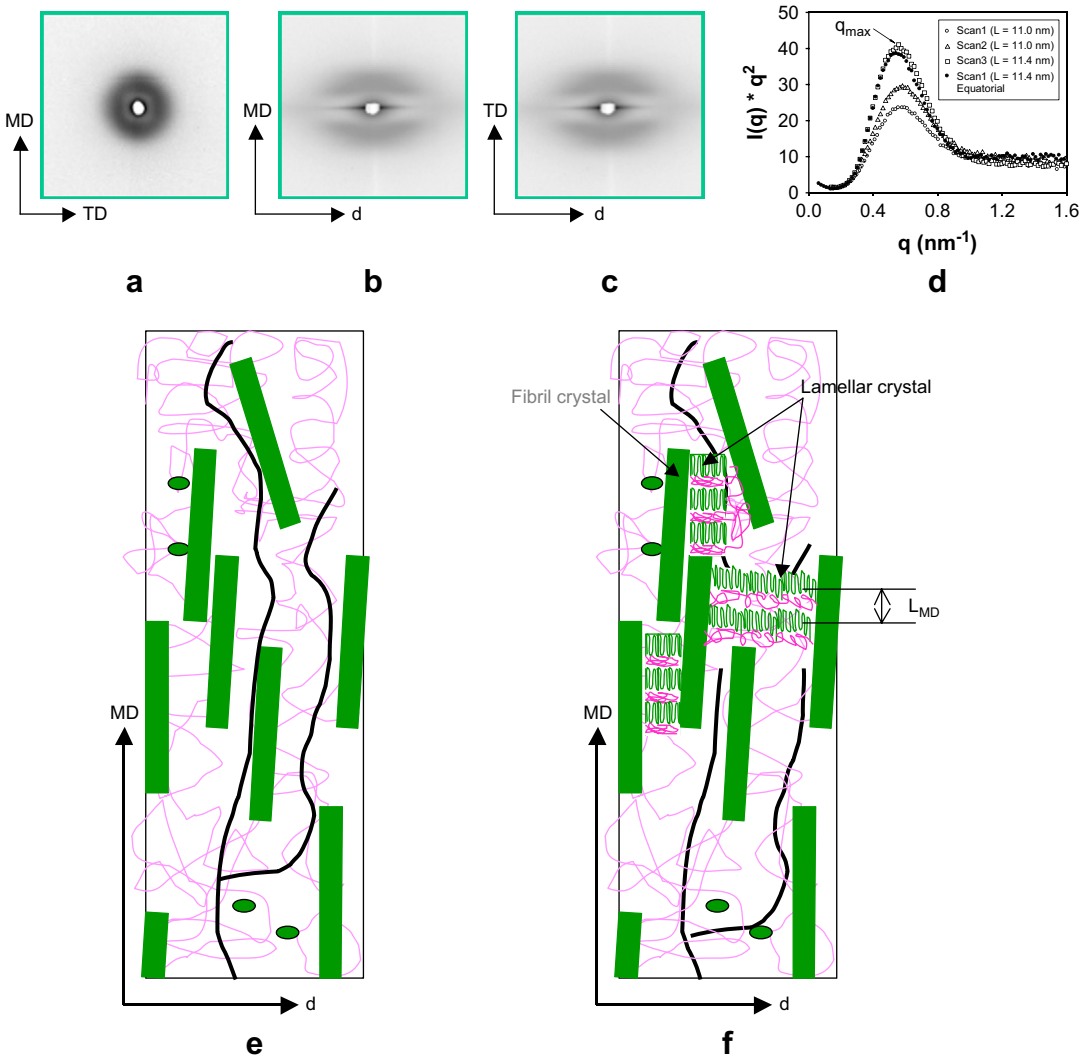

Fig. 8. Microstructure changes upon heatsetting; (a)–(c) SAXS patterns of heatset films: (a) SAXS pattern for *d*-direction incident (Scan 1); (b) SAXS pattern for TD incident (Scan 2); and (c) SAXS pattern of MD direction incident (Scan 3); (d) $I \sim q$ plot showing the ordering length in different scans; (e) and (f) illustrate microstructure before and after heatset: (e) microstructure of the MD–*d* plane showing fibril crystals and amorphous region before heatset and (f) microstructure of the MD–*d* plane after heatset showing the appearance of lamellar crystals perpendicular to the fibril crystals.

Fig. 7 illustrates the WAXD and SAXS patterns taken along the normal of the MD–*d* plane as well as a simplified microstructure model. The WAXD pattern (Fig. 7a) shows that the film is crystalline and highly oriented. The crystals have a preferred orientation in which the *c*-axis resides within the MD–TD plane, thus perpendicular to the thickness direction. According to the diffraction arc widths in Fig. 7b, the crystal size along the MD and TD directions is relatively large (i.e., narrower peak width) and that along the thickness direction is relatively small (i.e., broader peak width). The corresponding SAXS pattern (Fig. 7c) exhibits only an equatorial streak, suggesting the presence of extended-chain "fibrillar-like" morphology. Combining the above X-ray results, a simplified 3-D microstructure is illustrated in Fig. 7d and e. It is shown that the sheet-like fibril crystals are randomly distributed in the MD–TD plane, where amorphous chains connect these crystals. The microstructural change upon heatsetting of the films is summarized in Fig. 8. Fig. 8a–c illustrate the SAXS patterns when the X-ray beam is incident from different directions. A common feature can be observed in these patterns, i.e., the appearance of meridional scattering, which is absent in the film without heatsetting (Fig. 7c). The meridional SAXS peak is a characteristic of lamellar crystals and can be used to calculate the long period and lamellar thickness (when the degree of crystallinity is known). Fig. 8d shows the intensity profile of meridional scattering taken along different incident directions. It is interesting to see that Fig. 8a has a ring pattern while Fig. 8b and c have arc patterns, which are evidences of preferred orientation of lamellar crystals. Fig. 8d indicates that there are two long periods: one with a value of 11.4 nm and the other one of 11 nm. The pattern analysis suggests that this phenomenon can be attributed to two lamellar populations with two lamellar thicknesses. One group is formed from the crystals, whose *c*-axis is parallel to the TD direction, and the other group is formed from the crystals, whose *c*-axis is parallel to the MD direction. The minor difference in the long period (and lamellar thickness) is suspected to be caused by the draw ratio difference along the two directions in the biaxial stretching process. Again, the microstructure of heatset films is reconstructed based on the SAXS results and is illustrated in Fig. 8f. It shows that the lamellar crystals grow perpendicular to the MD–TD plane. The microstructure of the film without heatsetting is shown in Fig. 8e for comparison. Fig. 8e also illustrates a possible crack propagation path for the non-heatset films, where the crack finds its path in the amorphous region and around the sheet crystals. This hypothesis is consistent with microscopy observation that the PET film without heatset delaminates, i.e., fracturing in a layered fashion along the film plane. When the same crack propagation path is considered in a heatset

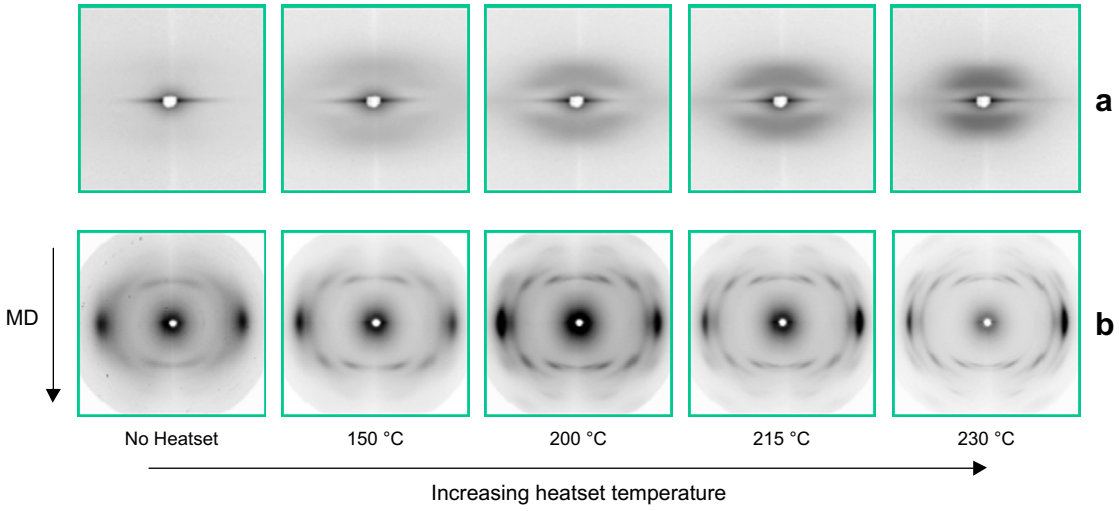

Fig. 9. Evolution of microstructure with heatset temperature: (a) SAXS and (b) WAXD.

film as shown in Fig. 8f, the crack propagation is usually stopped by the lamellar crystals formed during heatsetting, which is the mechanism for the increased toughness upon heatsetting (Fig. 5). The microstructural change upon different heatset temperatures is shown in Fig. 9. It is seen that the scattering intensity increases with increase in heatset temperature, suggesting an increase in the long-range order dimension and general increase in the number and size of secondary crystals. This can be explained as follows. At a certain heatset temperature, the secondary crystal can bridge adjacent crystal sheets. The further increase in heatset temperature does not change the nature of the secondary crystals. Overall, it is shown that the biaxial stretching process generates sheet-like "fibrillar" crystals dispersed within the biaxially oriented amorphous phase. When the film is heatset, some chain relaxation and loosening allow secondary crystals to form and grow perpendicular to the sheet-like primary crystals. At sufficiently high heatset temperatures, the secondary crystals can bridge adjacent primary sheet-like crystals and thereby alter the mechanical properties, especially the toughness, of the matrix. Under higher heatset temperatures, the primary crystals that are imperfect may begin to melt, although some secondary crystals may continue to grow under restrained conditions as shown in Fig. 4.

This structural model provides a reasonable explanation for the toughness dependence on the heatset temperature. As summarized in Fig. 10, it is suggested that the toughness of the semicrystalline film is determined primarily by the interconnectivity ("physical cross-linking") of the crystalline phase. The toughness can be maximized by creating a physical interpenetrating network comprising amorphous and crystalline domains. This general scheme could be applicable to any two-phase polymer system.

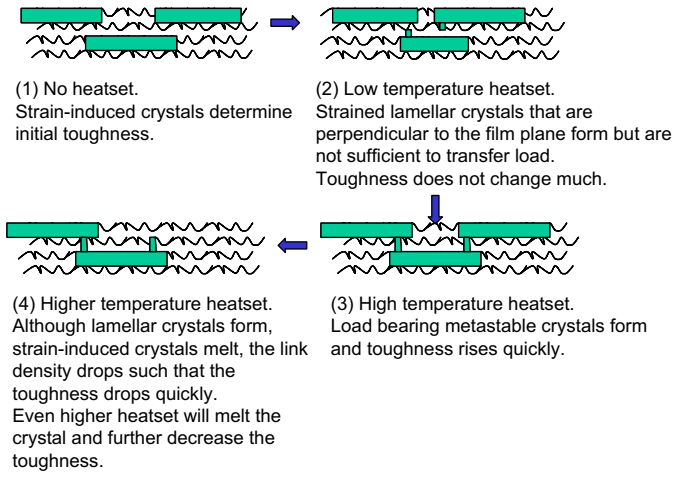

Fig. 10. A schematic summary of the evolving microstructure as a function of heatset temperature and its impact on the toughness of the film.

4. Conclusion

A biaxial stretching process was used to prepare optically transparent semicrystalline polyester films. The correlation between the microstructure and mechanical properties of the films was explored. The microstructure in the context of this study relates to the crystalline morphology and the degree of crystallinity of the semicrystalline film. By using a third comonomer, cyclohexane dimethanol (CHDM), PET-based films with similar crystalline morphology but different levels of crystallinity were produced and evaluated. By varying the heatset temperature it was possible to vary systematically the crystalline morphology of biaxially oriented PET films. These films were prepared by annealing under a lateral constraint at different temperatures below the nominal melting point. The tensile properties of the stretched and annealed polyester films were measured and correlated with their microstructure. Synchrotron SAXS and WAXD techniques were used to study the crystalline structure and morphology of the films; differential scanning calorimetry (DSC) was used to examine their thermal response. It is shown that the molecular structure of polyester chain as well as the process conditions used to fabricate the film can significantly impact the microstructure and the corresponding mechanical properties of the film. In particular, the results demonstrate the strong influence of microstructure on the ultimate properties, especially the toughness of the semicrystalline film. A microstructural model for the heatset PET films, invoking two types of crystals, fibrillar sheet crystals and lamellar crystals, was proposed. The connectivity and bridging of the primary crystals by the secondary ones appear to control the toughness and other ultimate properties of the film.

Acknowledgment

The authors thank Robert Kress and Beverly Contestable for their help with the experimental work. BH thanks the financial support from the National Science Foundation (DMR-0405432) with a Special Creativity Award.

References

[1] Hertzberg RW. Deformation and fracture mechanics of engineering materials. New York: John Wiley and Sons; 1976.
[2] Flory PJ. Principles of polymer chemistry. Ithaca: Cornell University Press; 1953.
[3] Young RJ, Lovell PA. Introduction to polymers. London: Chapman and Hall; 1991.
[4] Alexander LE. X-ray diffraction methods in polymer science. New York: Wiley-Interscience; 1969.
[5] Kawakami D, Hsiao BS, Burger C, Ran S, Avila-Orta C, Sics I, et al. Macromolecules 2005;38:91–103.
[6] Kawakami D, Ran S, Burger C, Avila-Orta C, Sics I, Chu B, et al. Macromolecules 2006;39:2909–20.
[7] Asano T, Balta-Calleja FJ, Flores A, Tanigaki M, Mina MF, Sawatari C, et al. Polymer 1999;40:6475–84.
[8] Keller A, Lester GR, Morgan LB, Hartley FD, Lord EW. Phil Trans R Soc A-1 1954; 247:13.
[9] Zachmann HG, Stuart HA. Makromol Chem 1960;41:131.
[10] Elsner G, Koch MHJ, Bordas J, Zachmann HG. Makromol Chem 1981;181:1263.
[11] Elsner G, Rickel C, Zachmann HG. Adv Polym Sci 1985;67:1.
[12] Guemther B, Zachmann HG. Polymer 1983;24:1008.
[13] Asano T, Zdeick-Pickuth A, Zachmann HG. J Mater Sci 1989;24:1967.
[14] Yeh GSY, Geil PH. J Macromol Sci B 1967;1:235.
[15] Yeh GSY, Geil PH. J Macromol Sci B 1967;1:251.
[16] Heffelfinger CJ, Schmidt PG. J Appl Polym Sci 1965;9(8):2661–80.
[17] G'Sell C, Marquez-Lucero A. Polymer 1993;34(13):2740–9.
[18] Chiu HC, Burns SJ, Fiscella MD, Benson RC. J Macromol Sci Phys 1994;B33(1): 87–104.
[19] Arkhireyeva A, Hashemi S. Plast Rubber Compos 2001;30(7):337–50.
[20] Maspoch ML, Henault V, Ferrer-Balas D, Velasco JI, Santana OO. Polym Test 2000;19:559–68.
[21] Arkhireyeva A, Hashemi S. J Mater Sci 2002;37:3675–83.
[22] Mocherla KKR, Statton WO. Appl Polym Symp Fiber Sci 1977;31:183–91.
[23] Hutchinson IJ, Ward IM, Willis HA, Zichy V. Polymer 1980;21(1):55–65.
[24] Gupta VB, Ramesh C, Siesler HW. J Polym Sci Polym Phys Ed 1985;23(2): 405–11.
[25] Clauss B, Salem DR. Macromolecules 1995;28(24):8328–33.
[26] Fischer EW, Fakirov S. J Mater Sci 1976;11:1041.
[27] Fakirov S, Fischer EW, Hoffmann R, Schmidt GF. Polymer 1977;18:1121.
[28] Nielsen LE, Landel RF. Mechanical properties of polymers and composites. New York: Marcel Dekker, Inc.; 1994.
[29] Greener J, Tsou AH, Blanton TN. Polym Eng Sci 1999;39(12):2403.
[30] Chang H, Schultz JM, Gohil RM. J Macromol Sci Phys 1994;B32:105.
[31] Lee K-G, Schultz JM. Polymer 1993;34:4455.
[32] Brandrup J, Immergut EH, Grulke EA. Polymer handbook. New York: John Wiley and Sons, Inc.; 1999.